Supporting Information

Electronic structure regulation induces highly efficient acidic OER in $RuIrTaO_x$

Wenou Bai*[ab], Ailing Yan[ab], Yucan Dong[ab], Jingai Wang[c], Bo Jia*[ab], Qing Feng[ab]

[a] *Xi'an Taijin New energy & Materials Sci-Tech Co. Ltd., Xi'an 710000, China.*

[b] *Northwest Institute for Non-ferrous Metal Research, Xi'an 710000, China.*

[c] *Xi'an Technological University, Xi'an 710000, China.*

E-mail: 15710489631@163.com

Characterization

The sample morphology was characterized using Scanning Electron Microscopy (SEM, JEOL) and Transmission Electron Microscopy (TEM, Talos F200S). The crystal structure characterization is performed using an X-ray diffractometer (XRD) with Cu Kα radiation. Surface chemical state analysis is performed using an X-ray photoelectron spectroscopy instrument (XPS, Thermo Fisher K-Alpha) with a high-performance monochromatic Al Kα (hν=1486.8 eV) radiation source. The metal content in the catalyst powder was analyzed using an Inductively Coupled Plasma Optical Emission Spectrometer (ICP-OES, Agilent 5100). Use the CHI660e electrochemical workstation from Chenhua for three-electrode system electrochemical testing. The oxygen vacancy uses an electron spin resonance spectrometer (EPR, Bruker A300). Electrolytic cell performance test using Guangzhou Qunyi Energy Co., Ltd. test bench.

$$D = \frac{K\lambda}{\frac{\beta}{180} \times 3.14 \times cos\theta} \cdots\cdots(1)$$

Scherrer formula

where D is the grain size, K is a constant, λ is the X-ray wavelength, β is the half-height width or integral height width of the peak, θ is the diffraction angle. In general, K is 0.89 when β is half-height width.

Electrochemical measurements

All electrochemical tests were conducted using carbon paper with an active area of 1 cm^2 as the working electrode. Prepare a homogeneous ink containing 5 mg of catalyst, 500 μL of ultrapure water, 500 μL of anhydrous ethanol, and 5 μL of Nafion. Take 100 μL of the homogeneous ink and evenly drop it onto both sides of a carbon paper measuring 1×1 cm^2. After drying, it can be utilized with a catalyst loading of 0.25 mg/cm^2. An Ag/AgCl electrode (with a standard hydrogen potential of 0.198 V, Gaoss Union 1060) was selected as the reference electrode (RE), and a Pt sheet electrode (measuring 1.5×1.5 cm^2, Gaoss Union) was utilized as the counter electrode (CE). The electrolyte is 0.5 M H_2SO_4. The linear sweep voltammetry (LSV) polarization curve test range spans from 0 to 2 V vs. RHE, with a scan rate of 100 mV/s. The polarization curve graph was plotted without IR compensation. Electrochemical impedance spectroscopy (EIS) was conducted at a voltage of 1.5 V vs. RHE, covering a frequency range from 10000 to 1 Hz. All test potentials are converted to hydrogen reference potential using equation (2), and the overpotential (η) is calculated using equation (3). The double-layer capacitance (C_{dl}) corresponding to the electrochemical active surface area (ECSA) is determined by analyzing

cyclic voltammetry (CV) curves obtained at testing potentials ranging from 0.7 V to 0.8 V vs. RHE and scan rates of 20, 40, 60, 80, and 100 mV/s. The difference between the upper and lower halves of the curve at a potential of 0.75 V vs. RHE is calculated, plotted against scan rate. The slope obtained from linear fitting of the scatter plot represents the C_{dl} value. The Tafel slope is determined by fitting a segment of the linear sweep voltammetry (LSV) curve at the initial section of the oxygen evolution reaction (OER).

$$E(vs\ RHE) = E(vs\ Ag\ /\ AgCl) + 0.198 + 0.0591 \times pH \cdots\cdots(2)$$

$$\eta(mV) = (E(vs\ RHE) - 1.23) \times 1000\cdots\cdots(3)$$

PEM electrolyser measurement

The membrane electrode assembly (MEA) was prepared by ultrasonic spraying method, using Chemus Nafion 115 proton exchange membrane without any treatment before spraying. The anode and cathode catalyst inks were composed of a quantitative catalyst powder, a water-alcohol mixture with a ratio of 3:7 of deionized water and isopropyl alcohol, and 10% Nafion solution (5 wt%). The content of iridium on the anode side was 1 mg/cm^2, and the content of Pt (Pt/C, 40 wt_{Pt}%) on the cathode side was 0.4 mg/cm^2. Among them, the anode catalyst content of RuO_2 MEA is 6 mg/cm^2. The experiment was carried out utilizing a PEM electrolyzer featuring an active surface area of 25 cm^2. Both anode and cathode side porous transport layer are composed of a 25 cm^2 platinum-coated titanium felt. The test temperature is 50 and 80 ℃. Each test point was stabilized for a duration of 60 s, and the average value of the last 30 s was considered as the data used for plotting the polarization curve. The stability test was carried out at 50℃.

DFT calculation

All first-principles calculations are performed using the plane-wave projector-augmented wave method, as implemented in the Vienna ab initio simulation package (VASP) [1, 2]. The Perdew−Burke−Ernzerhof (PBE) form of generalized gradient approximation (GGA) is chosen as the exchange−correlation potential [3]. The strong correlation effect of transition metal is addressed with the Hubbard U correction to density functional theory (DFT) (GGA+U). The Hubbard U value for Ru and Ir are 3.8 eV and 4.2eV. The energy cutoff of 520 eV was used for structural relaxation. k-Spacing was set to 0.4 for all structures to allow the smallest spacing between k-points in the unit of 0.4 Å^{-1}. The conjugated gradient method is utilized to optimize the geometry

with the convergence threshold of 10^{-5} eV in energy and 0.02 eV/Å in force, respectively.

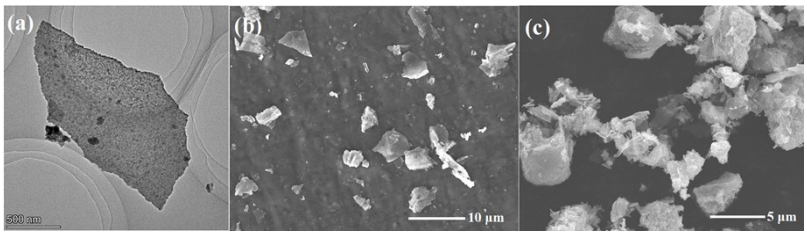

Figure S1 (a, b) TEM and SEM spectra of RuO_x; (c) SEM spectrum diagram of $RuIrO_x$

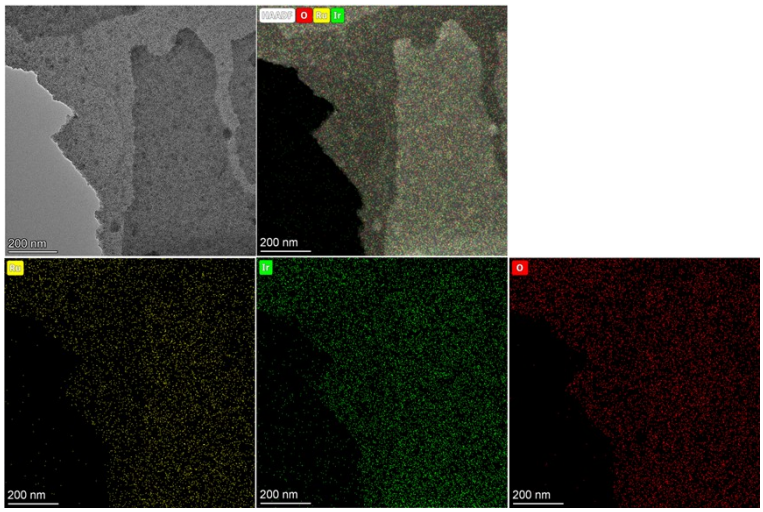

Figure S2 Mapping spectra of $RuIrO_x$

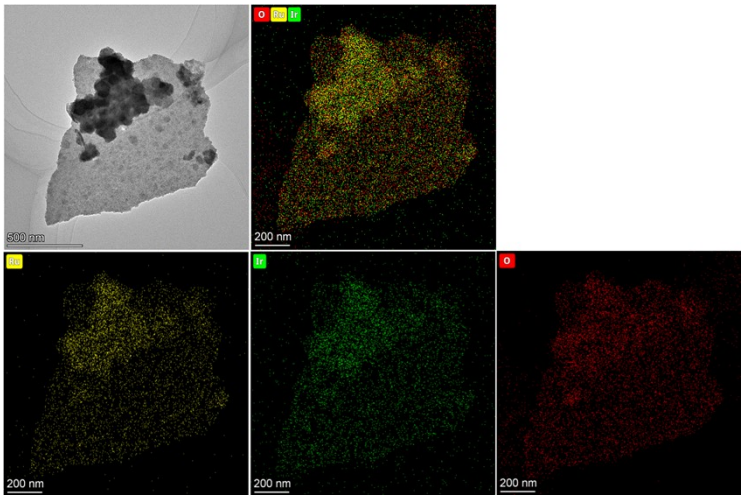

Figure S3 Mapping spectra of stack $RuIrO_x$

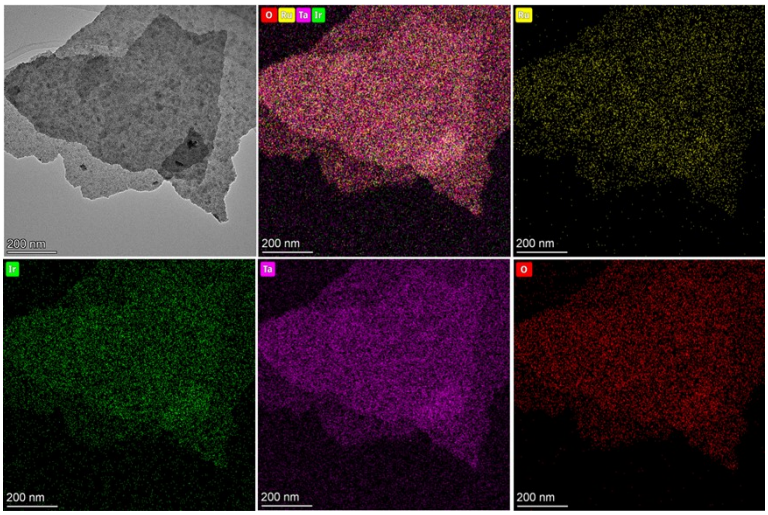

Figure S4 Mapping spectra of stack $RuIrTaO_x$

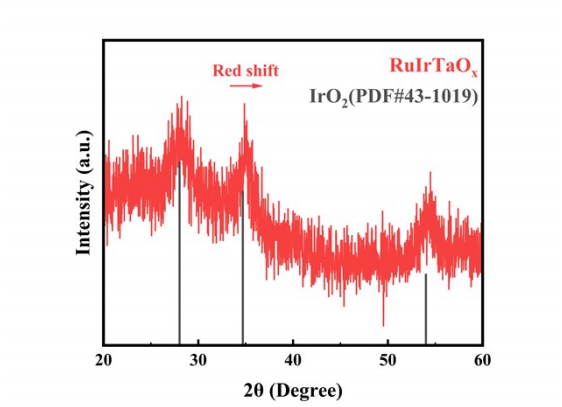

Figure S5 XRD pattern of $RuIrTaO_x$

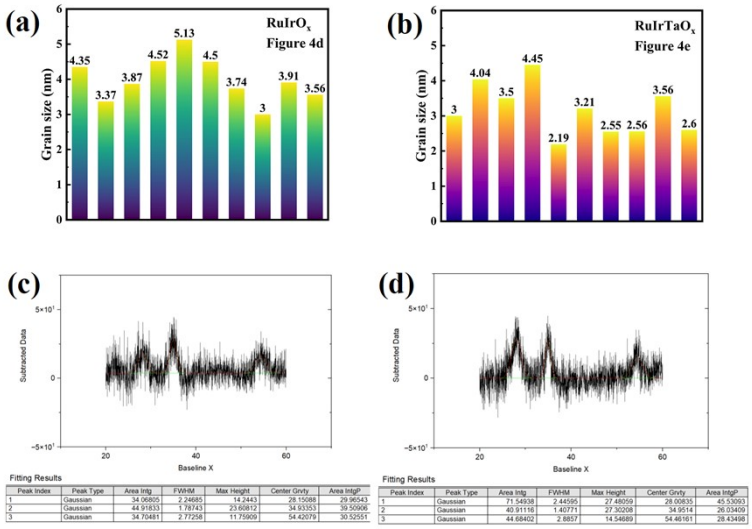

Figure S6 Grain size and XRD peak fitting spectra of $RuIrO_x$ (a and c) and $RuIrTaO_x$ (b and d)

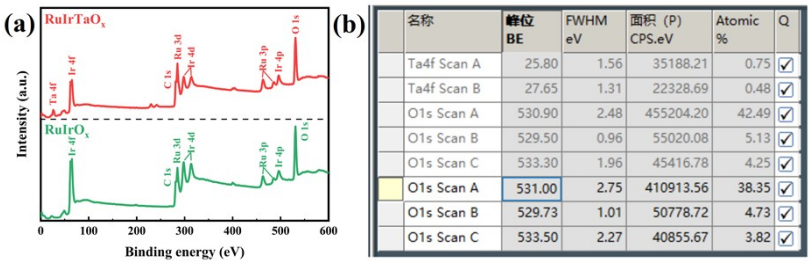

	名称	峰位 BE	FWHM eV	面积 (P) CPS.eV	Atomic %	Q
	Ta4f Scan A	25.80	1.56	35188.21	0.75	☑
	Ta4f Scan B	27.65	1.31	22328.69	0.48	☑
	O1s Scan A	530.90	2.48	455204.20	42.49	☑
	O1s Scan B	529.50	0.96	55020.08	5.13	☑
	O1s Scan C	533.30	1.96	45416.78	4.25	☑
	O1s Scan A	531.00	2.75	410913.56	38.35	☑
	O1s Scan B	529.73	1.01	50778.72	4.73	☑
	O1s Scan C	533.50	2.27	40855.67	3.82	☑

Figure S7 (a) XPS full spectrum of $RuIrO_x$ and $RuIrTaO_x$; (b) Peak fitting results of Ta 4f and O 1s high-resolution spectra

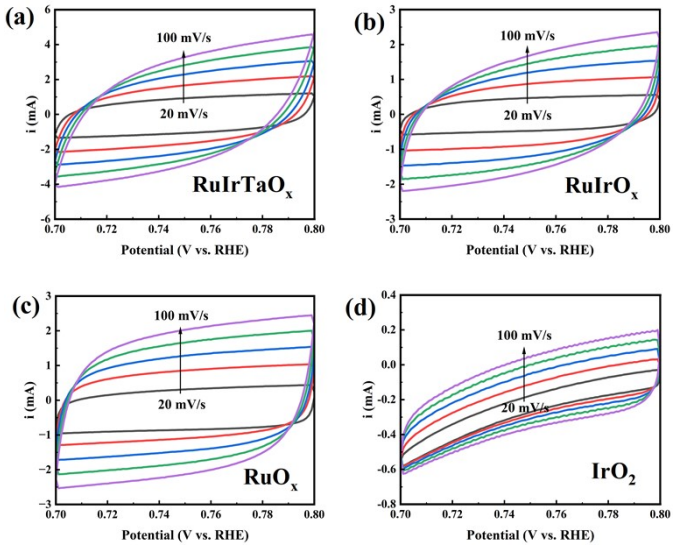

Figure S8 CV curves of (a) $RuIrTaO_x$, (b) $RuIrO_x$, (c)RuO_x and (d) IrO_2 at different sweep speeds (20-100 mV/s)

	A	B	C	D	E
1	Equation	y = a + b*x	y = a + b*x	y = a + b*x	y = a + b*x
2	Plot	B	C	D	E
3	Weight	No Weighting	No Weighting	No Weighting	No Weighting
4	Intercept	1.12556 ± 0.20547	0.49525 ± 0.14942	0.44121 ± 0.04339	0.01907 ± 0.00443
5	Slope	0.0528 ± 0.0031	0.02949 ± 0.00225	0.03758 ± 6.54101E-4	0.00391 ± 6.67992E-5
6	Residual Sum of Squares	0.11514	0.06089	0.00513	5.35456E-5
7	Pearson's r	0.99488	0.99136	0.99955	0.99956
8	R-Square (COD)	0.98978	0.9828	0.99909	0.99913
9	Adj. R-Square	0.98637	0.97706	0.99879	0.99883

Figure S9 Fitting parameter diagram of current value at 0.75V vs. RHE potential in CV curve at 20-100 mV/s sweep speed

	A	B	C	D	E
1	Equation	y = a + b*x			
2	Plot	B	D	F	H
3	Weight	No Weighting			
4	Intercept	1.40305 ± 7.26371E-5	1.39458 ± 1.53051E-4	1.39673 ± 1.30882E-4	1.5105 ± 7.07517E-4
5	Slope	0.07285 ± 1.69452E-4	0.09613 ± 3.62837E-4	0.08407 ± 5.11889E-4	0.10805 ± 0.00106
6	Residual Sum of Squares	7.14508E-7	1.32082E-6	3.43513E-6	1.58996E-5
7	Pearson's r	0.99991	0.99978	0.99943	0.99826
8	R-Square (COD)	0.99982	0.99956	0.99885	0.99652
9	Adj. R-Square	0.99981	0.99954	0.99881	0.99642

Figure S10 Fitting parameter diagram of Tafel slope

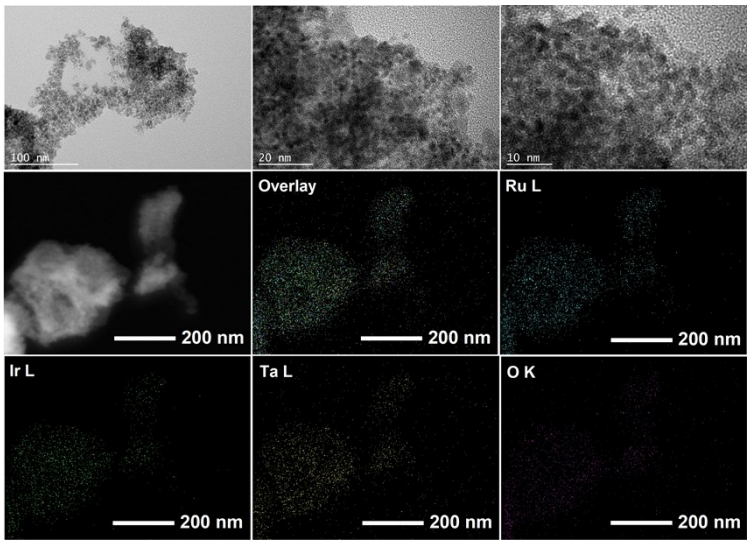

Figure S11 TEM and Mapping images after PEMWE stability test of $RuIrTaO_x$

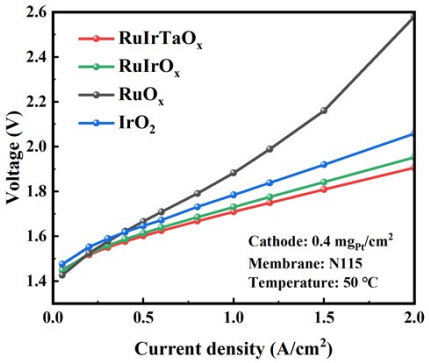

Figure S12 I-V curves of $RuIrTaO_x$, $RuIrO_x$, RuO_x and IrO_2 MEA tested in PEMWE at 50 °C

Table S1 Comparison between $RuIrTaO_x$ and current Ir-based catalysts

Sample	Electrolyte	η@10 mA/cm^2 mV	Tafel slope mV dec^{-1}	Mass activity@η=300 mV A/g_{pm}	PEMWE stability h	Ref.
$RuIrTaO_x$	0.5 M H_2SO_4	237	72.8	773.29 (1482.6 @350 mV)	500 @1000 mA/cm^2	This Work
$W_{0.7}Ir_{0.3}O_y$	0.1 M $HClO_4$	278	45.99	714.1	90 @500 mA/cm^2	4
IrO_x_NaCl	0.5 M H_2SO_4	350	42	/	/ /	5
$IrNiO_x$	0.5 M H_2SO_4	320	/	/	500 @1000 mA/cm^2	6
Ir/MnO_x	0.1 M $HClO_4$	238	42.5	/	300 @1000 mA/cm^2	7
$Ir\text{-}IrO_xH_ySe_z$	0.5 M H_2SO_4	308	79.54	282.6	350 @1000 mA/cm^2	8
Ir@RuO_2 IO/Ti felt-300	0.5 M H_2SO_4	204	72.8	/	250 @1000 mA/cm^2	9
IrRu NWs	0.5 M H_2SO_4	243	52.5	/	500 @1000 mA/cm^2	10
$T\text{-}0.24Ni/IrO_2$	0.1 M $HClO_4$	190	58.6	1110.5 @350 mV	500 @500 mA/cm^2	11
$IrO_x/Ir\text{-}WO_3$	0.5 M H_2SO_4	239	75.2	1600	40 @30 mA/cm^2	12
Ir_3Ni NCs	0.2 M $HClO_4$	282	44.9	3720 @350 mV	180 @100 mA/cm^2	13
ZnNiCoIrMn	0.1 M $HClO_4$	237	46	610.8 @270 mV	/ /	14
Ir-doped $CoMn_2O_4$	0.5 M H_2SO_4	232	54.5	3562	400	15

					@1000 mA/cm^2	
IrO_x NRs/Sb-SnO_2	0.1 M $HClO_4$	/	42	1512	/ /	[16]
H-IrO_x FPs	0.1 M $HClO_4$	262	42	/	2000 >1000 mA/cm^2	[17]
40%-Ir/B_4C	0.1 M $HClO_4$	285	39	1139.7 @310 mV	100 @2000 mA/cm^2	[18]
Ir/1-TiO_2	0.5 M H_2SO_4	288	54.4	240.13 @270 mV	/ /	[19]
IrO_2/TiO_2-1	0.5 M H_2SO_4	247	53.6	/	350 @1000 mA/cm^2	[20]
IrO_x@CM-100	0.5 M H_2SO_4	264	/	120.2 @264 mV	24 @1000 mA/cm^2	[21]
Ir_x@$Au_{0.25}Ir_{0.75-x}$	0.5 M H_2SO_4	235	56.1	248 @370 mV	100 @500 mA/cm^2	[22]
IrO_x/TiO_x	0.5 M H_2SO_4	233	55.1	730.8	220 @1000 mA/cm^2	[23]
IrO_x/Nb_4N_5	0.5 M H_2SO_4	247	53.2	/	250 @1000 mA/cm^2	[24]
Ir-3 MA	0.1 M $HClO_4$	270	43	740	1200 @500 mA/cm^2	[25]
Ir/Ta_2O_5	0.1 M $HClO_4$	288.2	44.1	876.1 @320 mV	48 @1000 mA/cm^2	[26]
40-Ir_2Ni/TiN	0.5 M H_2SO_4	267	52	1070 @320 mV	100 @500 mA/cm^2	[27]
J-IrNT	0.1 M $HClO_4$	391	71	1340 @370 mV	100 @200 mA/cm^2	[28]
IrO_x/Zr_2ON_2	0.5 M H_2SO_4	255	48	849 @320 mV	50 @1000 mA/cm^2	[29]

Table S2 The metal content in different catalysts measured by ICP-OES

Catalysts	Ru (wt%)	Ir (wt%)	Ta (wt%)
$RuIrO_x$	11.46	16.65	-
$RuIrTaO_x$	6.00	16.17	27.13

Reference

1. G. Kresse and J. Hafner, *Phys. Rev. B*, 1994, **49**, 14251-14269.
2. G. Kresse and J. Furthmüller, *Phys. Rev. B*, 1996, **54**, 11169.
3. J. P. Perdew, K. Burke and M. Ernzerhof, *Phys. Rev. Lett.*, 1996, **77**, 3865-3868.
4. T. Yan, S. Chen, W. Sun, Y. Liu, L. Pan, C. Shi, X. Zhang, Z.-F. Huang and J.-J. Zou, *ACS Applied Materials & Interfaces*, 2023, **15**, 6912-6922.
5. S. Kim, J. Woo, Y.-L. T. Ngo, H.-Y. Park, J. Y. Kim, J. H. Jang and B. Seo, *Small*, 2025, **n/a**, 2412083.
6. S. S. Jeon, H. Jeon, J. Lee, R. Haaring, W. Lee, J. Nam, S. J. Cho and H. Lee, *ACS Catalysis*, 2025, **15**, 4963-4974.
7. D. Wang, F. Lin, H. Luo, J. Zhou, W. Zhang, L. Li, Y. Wei, Q. Zhang, L. Gu, Y. Wang, M. Luo, F. Lv and S. Guo, *Nature Communications*, 2025, **16**, 181.
8. M.-G. Kim, H. J. Lee, T. K. Lee, E. Lee, H. Jin, J.-H. Park, S. Y. Cho, S. Lee, H. C. Ham and S. J. Yoo, *ACS Energy Letters*, 2024, **9**, 2876-2884.
9. Z. Wang, H. Yu, J. Na, J. Chi, S. Jia, J. Li and Z. Shao, *International Journal of Hydrogen Energy*, 2025, **114**, 97-105.
10. B. Pang, S. Feng, Y. Xu, H. Chen, J. Li, Y. Yuan, X. Zou, X. Tian and Z. Kang, *Advanced Functional Materials*, 2024, **34**, 2411062.
11. M. Liu, X. Zhong, X. Chen, D. Wu, C. Yang, S. Li, C. Ni, Y. Chen, Q. Liu and H. Su, *Advanced Materials*, 2025, **n/a**, 2501179.
12. Q. Wang, K. Zhang, Z. Zhang, X. Chen, H. Deng, W. Hua, J. Wei, S. Shen and J. Chen, *ACS Applied Materials & Interfaces*, 2025, **17**, 7929-7937.
13. H. Ding, C. Su, J. Wu, H. Lv, Y. Tan, X. Tai, W. Wang, T. Zhou, Y. Lin, W. Chu, X. Wu, Y. Xie and C. Wu, *Journal of the American Chemical Society*, 2024, **146**, 7858-7867.
14. J. Kwon, S. Sun, S. Choi, K. Lee, S. Jo, K. Park, Y. K. Kim, H. B. Park, H. Y. Park, J. H. Jang, H. Han, U. Paik and T. Song, *Advanced Materials*, 2023, **35**, 2300091.
15. W. Ko, J. Shim, H. Ahn, H. J. Kwon, K. Lee, Y. Jung, W. H. Antink, C. W. Lee, S. Heo, S. Lee, J. Jang, J. Kim, H. S. Lee, S.-P. Cho, B.-H. Lee, M. Kim, Y.-E. Sung and T. Hyeon, *Journal of the American Chemical Society*, 2025, **147**, 2369-2379.
16. G. Shi, T. Tano, D. A. Tryk, T. Uchiyama, A. Iiyama, M. Uchida, K. Terao, M. Yamaguchi, K. Tamoto, Y. Uchimoto and K. Kakinuma, *ACS Catalysis*, 2023, **13**, 12299-12309.
17. Z. Xie, H. Chen, X. Wang, Y. A. Wu, Z. Wang, S. Jana, Y. Zou, X. Zhao, X. Liang and X. Zou, *Angewandte Chemie International Edition*, 2025, **64**, e202415032.
18. J. Islam, S.-K. Kim, M. M. Rahman, P. T. Thien, M.-J. Kim, H.-S. Cho, C. Lee, J. H. Lee and S. Lee, *Materials Today Energy*, 2023, **32**, 101237.

19. P. Huang, X. Xu, Y. Hao, H. Zhao, X. Liang, Z. Yang, J. Yun and J. Zhang, *ACS Omega*, 2024, **9**, 34482-34492.

20. C. Yang, W. Ling, Y. Zhu, Y. Yang, S. Dong, C. Wu, Z. Wang, S. Yang, J. Li, G. Wang, Y. Huang, B. Yang, Q. Cheng, Z. Liu and H. Yang, *Applied Catalysis B: Environment and Energy*, 2024, **358**, 124462.

21. T. B. N. Huynh, D. Lee, S.-K. Kim, M. J. Kim and O. J. Kwon, *Journal of Materials Chemistry A*, 2023, **11**, 14221-14231.

22. H. Huang, T. Chen, D. Fang, L. Cao, G. Wang, J. Hao and Z. Shao, *Journal of Applied Electrochemistry*, 2024, **54**, 2269-2279.

23. Y. Qin, Y. Huang, Q. Ye, J. Wang, M. Endo, M. Dou and F. Wang, *Advanced Energy Materials*, 2025, **n/a**, 2405636.

24. X. Duan, H. Liu, W. Zhang, Q. Ma, Q. Xu, L. Khotseng and H. Su, *Electrochimica Acta*, 2023, **470**, 143271.

25. J. Liang, C. Fu, S. Hwang, C. Dun, L. Luo, Z. Shadike, S. Shen, J. Zhang, H. Xu and G. Wu, *Advanced Materials*, 2025, **37**, 2409386.

26. C. Baik, J. Cho, J. I. Cha, Y. Cho, S. S. Jang and C. Pak, *Journal of Power Sources*, 2023, **575**, 233174.

27. H. Lv, H. Yao, Y. Sun, D. Hu, Y. Gao, J. Chen and C. Zhang, *International Journal of Hydrogen Energy*, 2024, **84**, 634-640.

28. J. Kim, T. Kwon, J. Lee, H. J. Lee, M. Jun, H. C. Ham, H. Ju, S. Kim and J. Y. Kim, *Advanced Energy Materials*, 2024, **14**, 2400999.

29. C. Lee, K. Shin, Y. Park, Y. H. Yun, G. Doo, G. H. Jung, M. Kim, W.-C. Cho, C.-H. Kim, H. M. Lee, H. Y. Kim, S. Lee, G. Henkelman and H.-S. Cho, *Advanced Functional Materials*, 2023, **33**, 2301557.